Journal of The Electrochemical Society, **150** (9) E423-E428 (2003)
0013-4651/2003/150(9)/E423/6/$7.00 © The Electrochemical Society, Inc.

EIS Studies of Porous Oxygen Electrodes with Discrete Particles

I. Impedance of Oxide Catalyst Supports

Guoying Chen,[a] Chad C. Waraksa,[a] Hungoo Cho,[b] Digby D. Macdonald,[b,*,z] and Thomas E. Mallouk[a,]**

[a]*Department of Chemistry and* [b]*Department of Materials Science and Engineering, The Pennsylvania State University, University Park, Pennsylvania 16802, USA*

Two titanium oxide catalyst supports for the oxygen electrode of unitized regenerative fuel cells were compared by electrochemical impedance spectroscopy (EIS) techniques. One was a commercial Ebonex sample, which is a mixture of Ti_4O_7 and other conductive Magneli phases, and the other was a niobium-doped rutile oxide, $Ti_{0.9}Nb_{0.1}O_2$. Both supports were loaded with a mixed Ir-Ru-Pt oxide catalyst and conditioned anodically. The impedance spectra shows a resistive component which can be assigned, using transmission line modeling of the catalyst/support/electrode structure, to the series resistance of the support particles. Although both supports increase in resistance with anodic conditioning, the increase is greater for Ebonex. This increase in support resistance is consistent with oxidation of Ti^{III} to Ti^{IV}, which appears to be reversible in the case of the Nb-doped rutile material but irreversible with Ebonex.
 [DOI: 10.1149/1.1594729]

Manuscript submitted July 12, 2002; revised manuscript received March 6, 2003. Available electronically July 15, 2003.

Porous electrodes provide a large reactive surface area in a small volume, and they have a wide range of applications in modern electrochemistry, especially in fuel-cell and electrolyzer systems, where high utilization of noble metal catalysts at the anode and cathode of the cells is crucial. The well-known three-phase interactions of liquid electrolyte, solid catalyst, and gaseous reactant on porous catalyst electrodes is one of the most important phenomena in electrocatalysis, and a tremendous amount of research has been carried out to better understand the geometric and electronic characteristics of these electrodes.[1]

Electrochemical impedance spectroscopy (EIS) is a frequency-domain method that provides much more information about the system studied than steady-state techniques, since most processes that exhibit different relaxation times can be resolved in the frequency domain. These techniques have been successfully used to study metal dissolution and corrosion phenomena,[2] to measure kinetic parameters such as transfer coefficients, exchange current densities, heterogeneous rate constants for charge-transfer reactions, and to measure grain boundary thickness in polycrystalline solids.[3] EIS has also been used to study charge-transfer reaction mechanisms. A qualitative reaction model of the electro-oxidation of methanol on polished polycrystalline platinum was recently developed by Melnick and Palmore using a time-dependent impedance technique.[4]

The application of EIS to porous electrode studies has been hampered by the often difficult mathematical description of porous systems. The developed mathematical model must be sufficiently detailed to elucidate the complex geometric and electrochemical parameters of a porous ensemble. Early work on porous electrodes was focused on modeling to gain insight into their geometric properties.[5] Later, EIS was used to study faradaic processes in pores such as the oxygen reduction reaction in fuel cells.[6,7] Macdonald *et al.* studied the electrochemical reactions of porous nickel electrodes in battery systems.[8] They modified the classical transmission line model and devised an electrical/physical model for the solid-liquid interface in order to account for the measured interfacial impedance.[8] In their model, the three-dimensional problem was transformed into a one-dimensional model by dividing the porous interface into a finite number of segments and placing the resistance of the solid phase and the solution phase per unit length in the direction of the imposed current flux, with the interfacial impedance distributed in between. Subsequent mathematical analysis gave detailed information about the interface and the electrochemical process.

Recently, we reported the synthesis and characterization of bifunctional electrocatalysts, $Pt_4Ru_4Ir_1$, on conductive titanium oxide supports. The electrochemical characteristics of these catalysts as the porous oxygen electrodes in unitized regenerative fuel cells (URFCs),[9] where water is oxidized during the electrolysis mode and oxygen is reduced during the subsequent fuel-cell mode, were examined. It was found that catalysts supported on $Ti_{0.9}Nb_{0.1}O_2$ had better electrochemical stability than those supported on Ebonex, particularly at high anodic potentials and under oxygen gas-enriched conditions. These differences became much more significant after lengthy conditioning of the supported catalyst electrodes under conditions of oxygen evolution at 1600 mV.

Ebonex consists of several suboxides of TiO_2, collectively known as Magneli phases (Ti_nO_{2n-1}, $4 \leqslant n \leqslant 10$), and it has the most conductive compounds of the series, Ti_4O_7 and Ti_5O_9, as its main components. Unlike $Ti_{0.9}Nb_{0.1}O_2$, which retains the rutile structure after introduction of the Nb dopant, the conductive Ebonex is oxygen-deficient due to edge sharing of TiO_6 octahedra in crystallographic shear planes. It is known that Magneli phase oxides can be thermally oxidized to nonconductive TiO_2, and so it was hypothesized that electrochemical oxidation also increases the resistivity of support. Therefore, it appeared likely that the activity and stability differences observed in our supported catalysts were the results of the difference in iR drops of the support materials caused by electrochemical oxidation.

In this paper, we use EIS of porous catalytic electrodes to investigate their electrochemical stability as the oxygen electrodes in URFCs. Using a detailed physical model derived from SEM images of the support particles on the electrode surface, we are able to determine the effect of anodic and cathodic polarization on the real part of the impedance of the supports. These studies confirm the irreversible electrochemical oxidation of the Magneli phase supports under conditions of oxygen evolution.

Experimental

Preparation, conditioning, and dc steady-state testing of the electrodes.—Gas diffusion porous electrodes were prepared by painting catalyst inks onto Toray carbon paper disks (Electrochem, Inc.), a procedure that has been previously described in detail. The electrode was then used as the working electrode in a three-electrode gas diffusion half-cell, with Pt gauze as the counter electrode, re-

* Electrochemical Society Fellow.
** Electrochemical Society Active Member.
z E-mail: ddm2@psu.edu

versible hydrogen electrodes (RHEs) as the reference electrode, and a 0.5 M H_2SO_4 solution as the electrolyte. A dc potential of 1600 mV, controlled by an EG&G Princeton Applied Research Corp. model 363 potentiostat/galvanostat, was applied to the half-cell for 30 min to condition the electrode and to stabilize the current. The electrode was then tested for its water oxidation activity by measuring the currents in a potential window of 1200-1800 mV, with an increment of 30 mV per step. The half-cell was then supplied with oxygen feed gas, and the electrode was conditioned at 600 mV for 30 min. Currents were recorded from 1000 to 300 mV, with a step size of 30 mV, to test the oxygen reduction activity of the electrode. The tested catalyst electrode was then conditioned at 1600 mV for 7 h, with a continuous flow of Ar-purged 0.5 M H_2SO_4 supplied to the cell during the process. The i-V curves for water oxidation and oxygen reduction were recorded afterward. All electrodes had a geometric area of approximately 2.45 cm^2.

Scanning electron microscopy studies.—Scanning electron microscopy (SEM) images of the electrodes were collected at the Electron Microscope Facility at The Pennsylvania State University, using a JEOL-JSM 5400 microscope at 30 kV accelerating voltage. Particle size distributions were determined from the integrated microanalyzer for imaging and X-ray (IMIX) analysis, a program that was purchased from Princeton Gamma Technologies.

Electrochemical impedance spectroscopy.—The impedance spectra were recorded on a Solartron 1250 frequency response analyzer, in the frequency range between 10 kHz and 0.1 Hz. The appropriate dc bias was applied by using a Solartron 1286 potentiostat/galvanostat with an RHE reference electrode. A small-amplitude (10 mV) sinusoidal wave output was superimposed on the applied dc potential. Each electrode was measured five times over the entire frequency range to ensure the stability of the electrode during the process and to assess the reproducibility of the data.

Results and Discussion

Morphological characterization of the porous oxygen electrode.—A micrograph of an as-prepared $Pt_4Ru_4Ir_1$/Ebonex electrode is shown in Fig. 1a. The carbon paper backing has a fibrous texture and is covered by unevenly distributed catalyst particles. At the magnification of these images, the metal particles on the support are not discernible because of their small size (3-5 nm). The support particles are nonuniform in shape and size, but obey a lognormal distribution, as shown in Fig. 1b. The surface coverage of the electrode (a geometric area of 2.45 cm^2) was estimated to be 85%, which corresponds to an effective area of $A_e = 2.09\ cm^2$. Similar morphological characteristics were observed on the $Ti_{0.9}Nb_{0.1}O_2$-supported $Pt_4Ru_4Ir_1$ electrode.

Electrochemical impedance spectroscopy.—Impedance spectra of the supported catalyst electrodes were recorded in the oxygen evolution region, with an applied dc potential of 1600 mV and current densities (normalized to the geometric area) from 5 to 7 mA/cm^2, depending on the electrodes tested. Figure 2 shows typical Nyquist plots of the electrochemical impedance behavior of electrodes $Pt_4Ru_4Ir_1$/Ebonex, $Pt_4Ru_4Ir_1/Ti_{0.9}Nb_{0.1}O_2$, and the same electrodes after 7 h anodic conditioning.

The x axis and y axis represent the real part of the impedance (Z') and the imaginary part of the impedance (Z''), respectively. In general, the measured impedance spectra are depressed semicircles in the complex plane, and they do not show the "semicircle centered on the real axis" feature that is typically observed in systems that can be represented by a simple resistance-capacitance (RC) equivalent circuit.[10] The origin of the deviation is from the presence of inhomogeneities and porosity in the electrode, which gives rise to a frequency-dependent penetration depth for the ac wave.

From the spectra, the real impedance component at very high frequency ($f > 1$ kHz) was found to be almost constant from experiment to experiment, and from electrode to electrode. A small scatter in the data was observed at very low frequency ($f \rightarrow 0.1$ Hz), especially for the anodically conditioned $Pt_4Ru_4Ir_1$/Ebonex electrode, and this can be attributed to the perturbation introduced by the extensive period of oxygen gas evolution[11] on the rough porous electrodes.

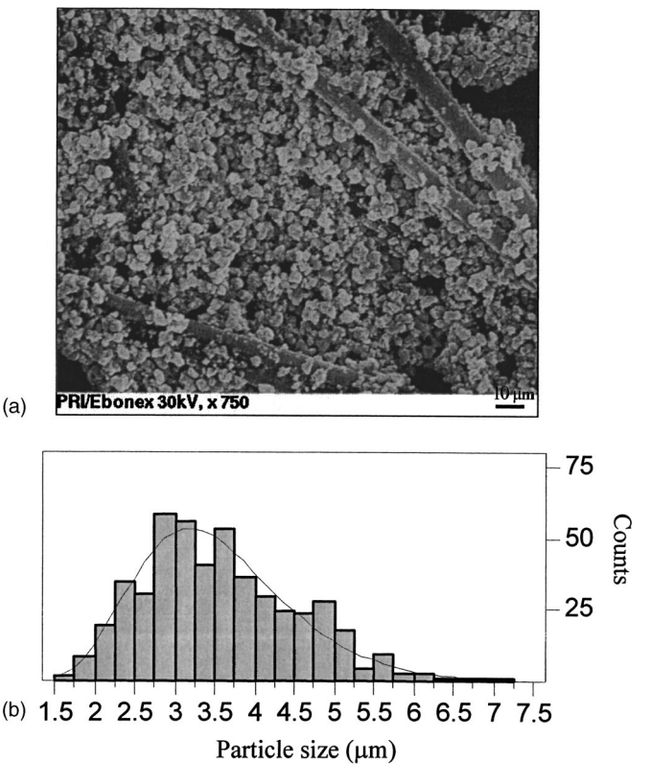

Figure 1. (a) SEM image of the Pt_4Ru_4 Ir_1/Ebonex electrode; (b) particle size distribution of the $Pt_4Ru_4Ir_1$/Ebonex catalyst base on a sample size of 494 particles.

According to the porous electrode model developed by Springer and Raistrick,[6a] the real component of the impedance at the very high frequency ($Z'_{f\rightarrow\infty}$) is the ionic resistance of the electrolyte together with all the external resistances, if applicable. The interfacial resistance at the very low frequency ($Z'_{f\rightarrow 0}$), which can be obtained by extrapolating the impedance spectrum to the real axis at limiting

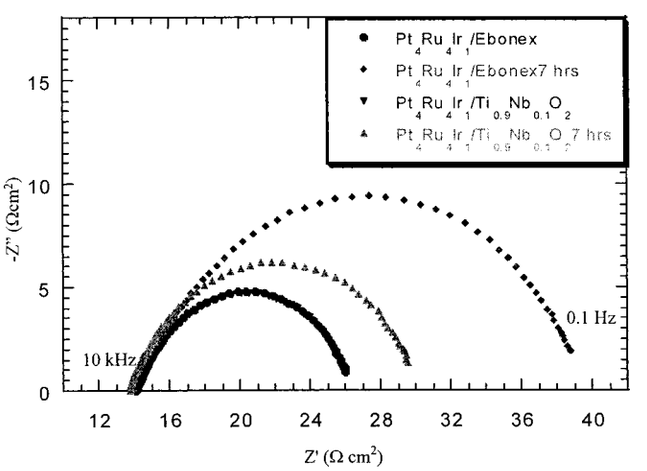

Figure 2. Nyquist plot of the ac impedance data of the indicated electrodes.

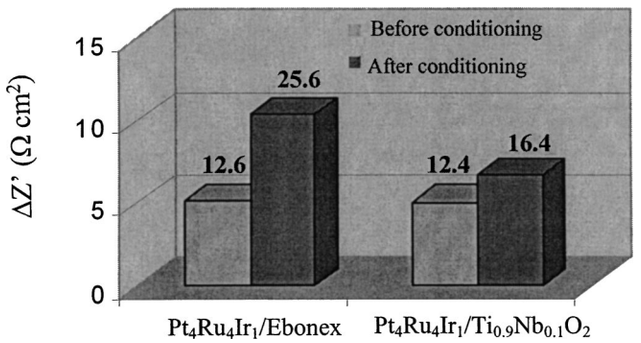

Figure 3. Electrochemical polarization resistance for the indicated electrodes.

low frequencies, represents the sum of the ionic contribution from the electrolyte (including the external resistances when present) and the electronic contribution from the electrode. The difference between the real part of impedances at extremely low and high frequencies ($\Delta Z'$), therefore, is the electrochemical polarization resistance (R_p), including the charge- and mass-transfer resistances across the porous catalyst electrode[2a,8a]

$$\Delta Z' = Z'_{f\to 0} - Z'_{f\to\infty} = R_p \qquad [1]$$

The impedance difference between high and low frequency for our catalytic porous electrodes is shown in Fig. 3. The $Pt_4Ru_4Ir_1$/Ebonex electrode had a polarization resistance of 12.6 Ω cm^2, while the same electrode after conditioning had a polarization resistance of 25.6 Ω cm^2. The polarization resistances for the $Pt_4Ru_4Ir_1/Ti_{0.9}Nb_{0.1}O_2$ electrode before and after conditioning were 12.4 and 16.4 Ω cm^2, respectively. These results show that electrochemical conditioning of the electrodes at 1600 mV increased their polarization resistances, and the $Pt_4Ru_4Ir_1$/Ebonex electrode was more sensitive to the process than the $Pt_4Ru_4Ir_1/Ti_{0.9}Nb_{0.1}O_2$ electrode.

Typical Bode plots of $\log|Z|$ *vs.* $\log f$, and phase angle *vs.* $\log f$ are shown in Fig. 4, where $|Z|$ is the impedance magnitude, f is the frequency, and the phase angle is the arctangent of the ratio of the imaginary and real parts of the measured impedance. At very high and low frequencies, the phase angles for all the electrodes were close to zero, which indicates the purely resistive nature of the system at these frequency limits. At intermediate frequencies, the electrodes, prior to the lengthy conditioning process, had phase angle values of about 13°, indicating the presence of reactance. The values increased as a result of electrode conditioning, with the conditioned $Pt_4Ru_4Ir_1$/Ebonex electrode reaching the highest value of 21°. Thus, long-term electrode conditioning increased the overall reactance of the electrodes at intermediate frequencies.

For each electrode, the impedance data were recorded several times in the indicated frequency range, and all the plots were virtually identical. This indicates that system was stable and the data were reproducible.

Modeling of the porous oxygen electrode.—Physical model.—A physical model of the porous oxygen electrodes was developed[12] based on the morphology observed in the SEM images. The following assumptions were used to render the mathematics tractable: (*i*) the support particles, Ebonex or $Ti_{0.9}Nb_{0.1}O_2$, were approximated as spherical; (*ii*) metal particles, with a composition of $Pt_4Ru_4Ir_1$, were evenly dispersed on the surface of the support spheres and were treated as part of the support wall; and (*iii*) the diameters of the catalyst/support spheres were the same as the length of the support particles, l, which was log-normally distributed as described. Current was assumed to have to pass through catalyst particles in order

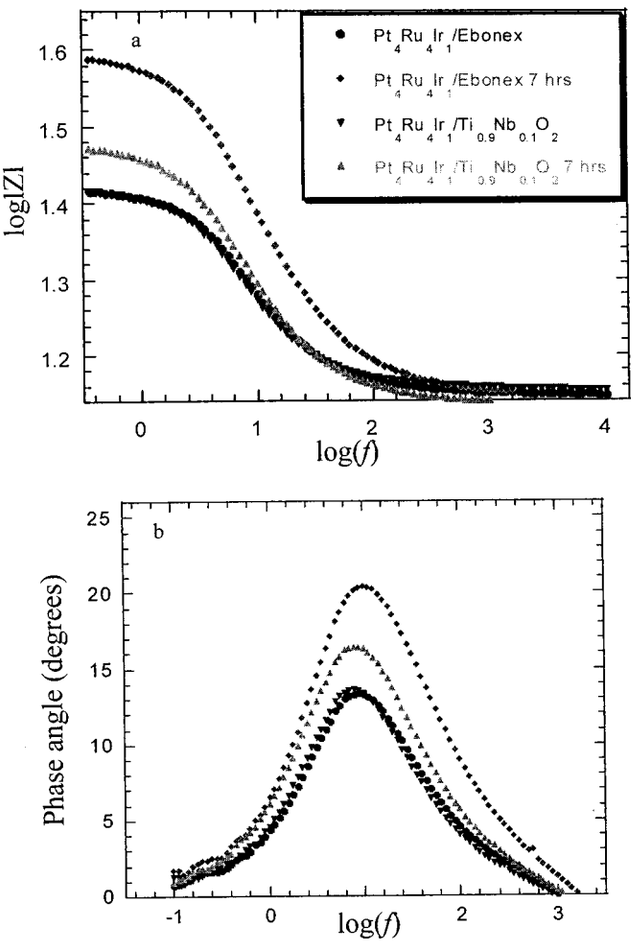

Figure 4. Bode plots of the ac impedance data of the indicated electrodes: (a) $\log|Z|$ *vs.* $\log f$; (b) phase angle *vs.* $\log f$.

to complete the electric circuit during electrochemical reactions, and it could only pass to the backing material where the carbon paper and the catalyst spheres were intimately touching.

Electric transmission line model.—The porous nature of our catalyst electrode suggests a transmission line model to describe the physical phenomena occurring during the water oxidation process. In most cases, a transmission line model simulates the impedance of one single representative or average pore by dividing the pore into N segments. Each segment has its impedance consisting of the resistance from the solution in the pores, the resistance from the electronically conducting solid phase, and the impedance from the pore walls. The mathematical details of the transmission line model are described elsewhere.[2,3,8]

In our porous oxygen electrodes, catalyst particles were dispersed as a multilayer on the carbon support surface, which led to poorly defined and nonuniformly distributed interstices. It is much simpler to model the electrode as hexagonal packing of spheres instead of as a random collection of particles forming irregular pores. Figure 5b shows the equivalent electrical circuit of a hexagonal unit cell of such spheres in discretized form, where R_e (Ω) is the external resistance including the uncompensated resistance between working and reference electrodes, V (V) is the applied voltage, $R_{m,k}$ (Ω) and $R_{s,k}$ (Ω) are the resistances per segment of the solid support material and the solution between the pores, respectively, Z_k (Ω) is the interfacial impedance per segment along the wall of the pore, Z' (Ω) is the interfacial impedance at the base of the

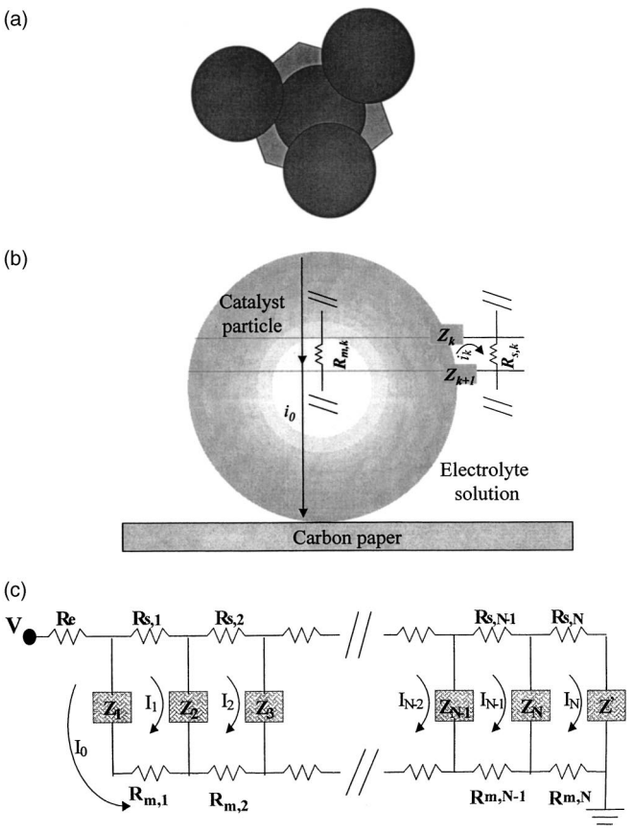

Figure 5. (a) A physical model of solid-liquid interface defined by one hexagonal unit cell with two layers of spheres; (b) segmentation of the interface; and (c) transmission line model for one unit cell.

hexagonal unit cell, and i (A) is the current that flows though the interface. The impedance of the porous electrode, Z_p (Ω), is calculated as a function of ten parameters

$$Z_p = f(\rho_m, \rho_s, R_w, C_w, R_{surf}, C_{surf}, R_e, f, n_{avg}, \omega) \qquad [2]$$

where the new terms are the resistivity of the catalyst support material ρ_m (Ω cm), solution resistivity ρ_s (Ω cm), the specific resistance and capacitance associated with the solution/pore wall interface R_w (Ω cm^2) and C_w (F/cm^2), the specific resistance and capacitance associated with the solution/carbon-paper interface R_{surf} (Ω cm^2) and C_{surf} (F/cm^2), and the angular frequency of the applied potential ω (rads/s). The terms f and n_{avg} represent a geometric sphere separation factor and the average number of layers of catalyst support particles.[12]

In our system, the concentration of the electrolyte was kept constant by using a continuous flow of 0.5 M H_2SO_4, and the resistivity of the electrolyte solution had a fixed value of 4.46 Ω cm.[13]

Initial simulation studies found that the ratios of the resistive terms are the most important factor in controlling the shape of the calculated impedance data. The distorted semicircle observed in our experiments can only be generated when ρ_c is large enough to not be dominated by the other variables in the system. Physically, this means that the porous nature of the electrode can only be observed when the resistivity of the catalyst, the solution, and the base are in the right proportion, which results in the current passing through both pathways of the segment loops and loop 0 in the transmission line model (Fig. 5b).

Figure 6 shows Nyquist and Bode plot fits between the predicted and the experimental impedance data collected on $Pt_4Ru_4Ir_1$/Ebonex electrode. Similar fits were obtained for the other

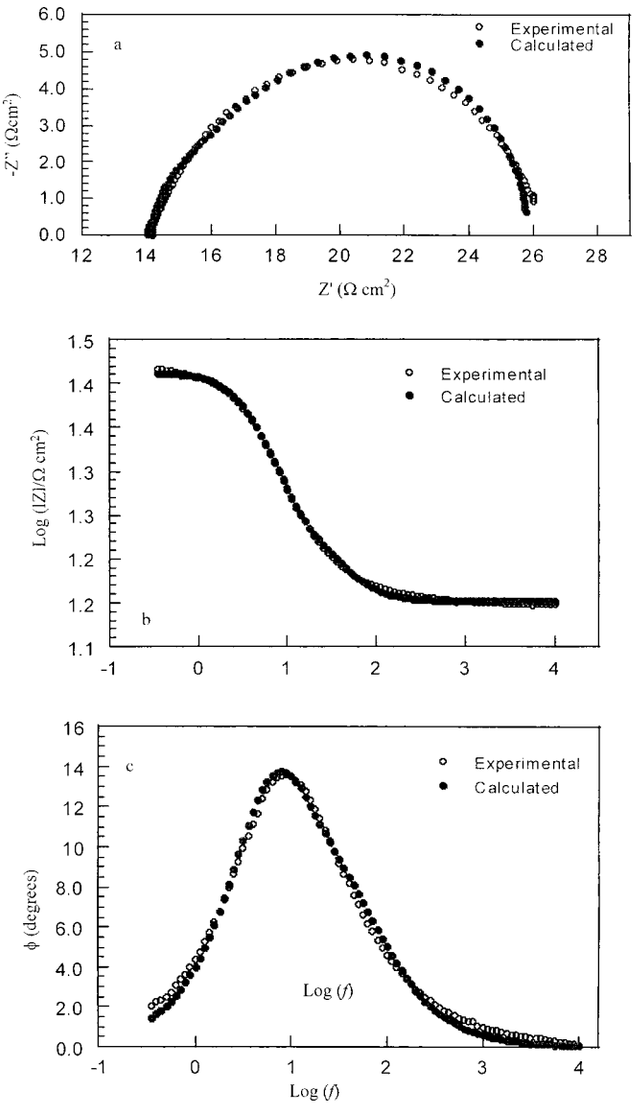

Figure 6. Curve-fitting of the calculated and experimental impedance data of the $Pt_4Ru_4Ir_1$/Ebonex electrode: (a) Nyquist plot fit of the real and imaginary parts of the impedance; (b) Bode plot fit of the impedance amplitude *vs.* frequency; and (c) Bode plot fit of the phase angles *vs.* frequency.

electrodes. The parameters derived from the curve fitting indicated that the two electrodes, after the initial 30 min conditioning, had very similar electrical characteristics, while the electrodes after a further 7 h conditioning showed major differences.

The optimized catalyst resistivities were $(5.7 \pm 1.1) \times 10^3$ Ω cm for the $Pt_4Ru_4Ir_1$/Ebonex electrode and $(5.7 \pm 1.1) \times 10^3$ Ω cm for the $Pt_4Ru_4Ir_1/Ti_{0.9}Nb_{0.1}O_2$ electrode, which were significantly larger than the resistivities measured on the as-prepared electrodes (1.7 and 4.0 Ω cm, respectively). After 7 h conditioning, the resistivities of both electrodes further increased, with the former reaching $(1.7 \pm 0.3) \times 10^4$ and the latter increasing to $(1.4 \pm 0.4) \times 10^4$ Ω cm.

These impedance results are consistent with our previous observations of the effects of conditioning on the anodic and cathodic polarization curves of the catalytic electrodes.[9] During the first 30 min of anodic half-cell conditioning, the freshly prepared electrodes are very sensitive to the applied anodic potential. The current drops quickly at first and then gradually stabilizes. The two electrodes have similar performance for water oxidation after conditioning at

Table I. The resistances of the particle, the wall interface, the base interface, and the solution (Ω) for the indicated electrodes.

	$Pt_4Ru_4Ir_1$ /Ebonex	$Pt_4Ru_4Ir_1$ /Ebonex 7 h	$Pt_4Ru_4Ir_1$ /$Ti_{0.9}Nb_{0.1}O_2$	$Pt_4Ru_4Ir_1$ /$Ti_{0.9}Nb_{0.1}O_2$ 7 h
Catalyst particle	6.7 ± 1.2	17.5 ± 2.6	6.87 ± 1.3	15.7 ± 3.4
Wall	4.00 ± 0.31 × 10^5	4.02 ± 0.31 × 10^5	4.09 ± 0.35 × 10^5	4.14 ± 0.41 × 10^5
Base	117 ± 1	265 ± 4	118 ± 2	163 ± 2
Solution[a]	0.0033	0.0026	0.0032	0.0030

[a] Solution resistance was calculated from the known resistivity of the electroloye.

1600 mV for 30 min, with the $Pt_4Ru_4Ir_1$ /$Ti_{0.9}Nb_{0.1}O_2$ electrode being slightly more active. After the additional lengthy conditioning at 1600 mV, both electrodes have increased resistivities, but the Ebonex-supported electrode becomes more resistive than the $Ti_{0.9}Nb_{0.1}O_2$-supported electrode. In the polarization curves, this is manifested as a decreased current at the same applied potential on both electrodes after the treatment, where the change in the $Pt_4Ru_4Ir_1$ /Ebonex electrode is more significant than the other electrode.

When these electrodes were tested in the subsequent oxygen reduction mode, more distinct differences were observed. Compared to the $Pt_4Ru_4Ir_1$ /Ebonex electrode, the $Pt_4Ru_4Ir_1$ /$Ti_{0.9}Nb_{0.1}O_2$ electrode had much better performance for the reaction after 30 min conditioning. It also showed nearly the same level of catalytic activity for oxygen reduction after extensive conditioning at 1600 mV, while the conditioned Ebonex-supported electrode had significant current drops.

In the titanium ceramics, the conductivity originates from the presence of the Ti^{III} species.[14] The Ti^{III} ion is very reactive and can be oxidized to Ti^{IV} under oxidizing conditions, such as a high-applied anodic potential[15]

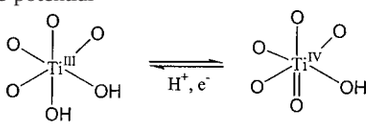

In $Ti_{0.9}Nb_{0.1}O_2$, Ti^{III} ions are generated by charge compensation of Nb^V, and they are present in the same rutile lattice as the Ti^{IV} ions. The oxidation process does not involve changes in the oxygen lattice; instead, oxidation of Ti^{IV} to Ti^{III} involves loss of protons from the surface of the particles, and it is reversible. This means that the Ti^{III} ions that are oxidized during the water oxidation process can be regenerated during the subsequent reverse reaction (oxygen reduction), and the electrode activity for oxygen reduction remains nearly the same after conditioning and cycling.

However, on the Ebonex support, the Ti^{III} ion is present in the Magneli phases, in which oxygen vacancies in the rutile structure are ordered into shear planes. The oxidation of the Ti^{III} ion in these phases decreases the oxygen deficiency in the structures and generates an undoped rutile lattice that is thermodynamically more stable. Therefore the process is irreversible. This was observed experimentally as the decreased activity of the $Pt_4Ru_4Ir_1$ /Ebonex electrode for both water oxidation and oxygen reduction after conditioning and cycling.

The derived specific resistances of the wall were (5.8 ± 0.5) × 10^4 Ω cm^2 for the $Pt_4Ru_4Ir_1$ /Ebonex electrode, and (5.9 ± 0.5) × 10^4 Ω cm^2 for the $Pt_4Ru_4Ir_1$ /$Ti_{0.9}Nb_{0.1}O_2$ electrode. The electrodes after the additional 7 h conditioning retained the same wall specific resistances. This indicated that lengthy conditioning after the initial period had little or no effect on the resistivity of the metal particles and the exterior wall of the support material. Because the wall is exposed to the solution, it can be understood that this material was completely oxidized during the initial conditioning period and became relatively inert afterward. The lengthy conditioning had a large effect on the interior of the support and greatly increased the resistivity of the catalyst particle, as discussed earlier.

The capacitances of the wall were 2500 ± 300 and 2700 ± 300 μF/cm^2 for the Ebonex- and $Ti_{0.9}Nb_{0.1}O_2$-supported catalyst electrodes, respectively. These values were based on the geometric area of the electrode. The measured Brunauer-Emmett-Teller (BET) surface area of the supported catalysts was 11.2 m^2/g,[9] which indicated a roughness factor of approximately 100 for the electrodes. By normalizing to this factor, the wall capacitance was found to be in the range of typical electric double-layer capacitance, commonly on the order of 10-100 μF/cm^2.[16]

After conditioning, the wall capacitances of the two electrodes decreased to 2300 ± 300 and 1500 ± 200 μF/cm^2, respectively. This was possibly due to the extension of the less conductive oxide layer to the interior from the support wall. The increased separation distance of the capacitor plates generated by this less conductive oxide shell and the interior of the support decreased the oxides' interface capacitance, which is in series with the catalyst-solution capacitance and is part of the overall wall capacitance.

The base specific resistances were 7.5 ± 0.1 and 7.3 ± 0.1 Ω cm^2 for the $Pt_4Ru_4Ir_1$ /Ebonex electrode and the $Pt_4Ru_4Ir_1$ /$Ti_{0.9}Nb_{0.1}O_2$ electrode, respectively. The extensive conditioning increased the resistances of electrodes to 17.1 ± 0.3 and 10.5 ± 0.2 Ω cm^2, but overall these values are much smaller than the wall specific resistances.

The resistances of the catalyst particle, the wall, the base, and the solution were calculated based on the optimized resistivities (or specific resistances) and surface geometry and are listed in Table I. In the current pathway of segment loops, a large ratio of wall resistance to the base resistance obtained in our system means that current is forced to enter the catalyst particle as close to the base segment as possible (Fig. 7), which physically leads to low utilization of the catalysts. Therefore, the design of more efficient catalyst systems is possible by largely decreasing this resistance ratio, by either decreasing the wall resistance or increasing the base resistance.

Similar to the observations on the wall capacitance, the base

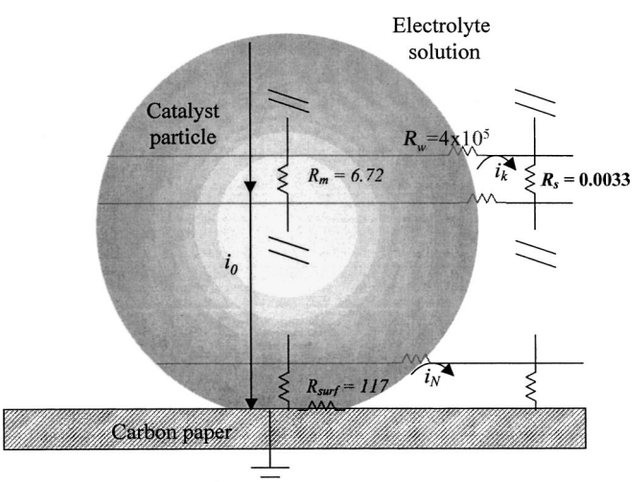

Figure 7. The resistance components (Ω) of each segment on the $Pt_4Ru_4Ir_1$ /Ebonex electrode.

capacitances of both electrodes decreased after lengthy conditioning, and the $Pt_4Ru_4Ir_1$/Ebonex showed a higher sensitivity to the process than the $Pt_4Ru_4Ir_1/Ti_{0.9}Nb_{0.1}O_2$ electrode.

All the electrodes had very similar external resistance, in the range of 10.7-12.2 Ω cm^2 after normalization to the geometric surface area, which reasonably agreed with the obtained experimental data ($Z'_{f\to\infty} \approx 13\ \Omega\ cm^2$).

Conclusions

The performance of two supported catalysts as the porous oxygen electrodes for URFCs was compared before and after an extensive conditioning period. Their electrochemical activities and stabilities were examined by EIS. Curve fitting of the impedance data by means of a transmission line model gave insight into the nature of the oxidative conditioning process and the observed differences in steady-state polarization behavior between Nb-doped TiO_2 and Magneli phase supports. In both cases, the resistance of the support is increased by anodic conditioning, consistent with the loss of conductivity that attends conversion of Ti^{III} to Ti^{IV}. Modeling showed that the increase in series resistance leads to lower catalyst utilization. In the case of the Nb-doped TiO_2 support, the increase in resistance appears to be reversible. This leads to a greater difference in performance between the two support materials at cathodic potentials, where oxygen is reduced.

Acknowledgments

This work was supported by a grant from the Army Research Laboratory, Collaborative Technology Alliance in Power and Energy, and by the U.S. Department of Energy through grant DE-FG02-01ER 15238. We thank Atraverda, Limited, for supplying Ebonex. Ebonex is a registered trademark of Atraverda, Limited.

The Pennsylvania State University assisted in meeting the publication costs of this article.

References

1. (a) E. W. Justi and A. W. Winsel, *J. Electrochem. Soc.*, **108**, 1073 (1961); (b) F. G. Will, *J. Electrochem. Soc.*, **110**, 145 (1963); (c) J. A. Rockett and R. Brown, *J. Electrochem. Soc.*, **113**, 207 (1966); (d) R. Brown and J. A. Rockett, *J. Electrochem. Soc.*, **113**, 865 (1966); (e) J. Giner and C. Hunter, *J. Electrochem. Soc.*, **116**, 1124 (1969).
2. (a) J. R. Park and D. D. Macdonald, *Corros. Sci.*, **23**, 295 (1983); (b) D. D. Macdonald and M. C. H. McKubre, in *ASTM Symposium on Electrochemical Techniques in Corrosion Science*, San Francisco, CA, May 1979.
3. J. Fleig, P. Pham, P. Sztulzaft, and J. Maier, *Solid State Ionics*, **113**, 739 (1998).
4. R. E. Melnick and G. T. R. Palmore, *J. Phys. Chem. B*, **105**, 1012 (2001); (b) R. E. Melnick and G. T. R. Palmore, *J. Phys. Chem. B*, **105**, 9449 (2001).
5. (a) R. de Levie, in *Advances in Electrochemistry and Electrochemical Engineering*, P. Delahay and C. T. Tobias, Eds. Vol. 6, p. 329, Interscience, New York (1967); (b) B. A. Boukamp, *Solid State Ionics*, **20**, 31 (1986); (c) R. de Levie, *Electrochim. Acta*, **10**, 113 (1965); (d) H. Keiser, K. D. Beccu, and M. A. Gutjahr, *Electrochim. Acta*, **21**, 539 (1976); (e) J.-P. Candy, P. Fouilloux, M. Keddam, and H. Y. Takenout, *Electrochim. Acta*, **26**, 1029 (1981); (f) J.-P. Candy, Pl. Fouilloux, M. Keddam, and H. Y. Takenout, *Electrochim. Acta*, **27**, 1585 (1982); (g) C. Cachet, P. de Pauli, and R. Wiart, *Electrochim. Acta*, **29**, 145 (1984); (h) C. Cachet and R. Wiart, *Electrochim. Acta*, **30**, 719 (1985).
6. (a) T. Springer and I. Raistrick, in *Electrode Materials and Processes for Energy Conversion*, S. Srinivasan, S. Wagner, and H. Wroblowa, Editors, PV 87-12, p. 152, The Electrochemical Society Proceedings Series, Pennington, NJ (1987); (b) A. S. Aricò, V. Alderucci, V. Antonucci, S. Ferrara, V. Recupero, N. Giordano, and K. Kinoshita, *Electrochim. Acta*, **37**, 523 (1992); (c) I. D. Raistrick, *Electrochim. Acta*, **35**, 1579 (1990).
7. (a) J. J. Coleman, *Trans. Am. Electrochem. Soc.*, **90**, 545 (1946); (b) S. Atlung and T. Jacobsen, *Electrochim. Acta*, **21**, 575 (1976); (c) H.-K. Song, H.-Y. Hwang, K.-H. Lee, and L. H. Dao, *Electrochim. Acta*, **45**, 2241 (2000).
8. (a) S. J. Lenhart, C. Y. Chao, and D. D. Macdonald, in *Proceedings of the 16th Intersociety Energy Conversion Engineering Conference*, ASME, New York, p. 663 (1981); (b) S. J. Lenhart, D. D. Macdonald, and B. G. Pound, *J. Electrochem. Soc.*, **135**, 1063 (1988); (c) S. D. Bhakta, D. D. Macdonald, B. G. Pound, and M. Urquidi-Macdonald, *J. Electrochem. Soc.*, **138**, 1353 (1991); (d) D. D. Macdonald, M. Urquidi-Macdonald, S. D. Bhakta, and B. G. Pound, *J. Electrochem. Soc.*, **138**, 1359 (1991).
9. G. Chen, S. R. Bare, and T. E. Mallouk, *J. Electrochem. Soc.*, In press.
10. (a) D. D. Macdonald and M. C. H. McKubre, *ASTM Spec. Tech. Publ.*, **727**, 110 (1981); (b) D. A. Denton, J. A. Harrison, and R. I. Knowles, *Electrochim. Acta*, **26**, 1197 (1981).
11. (a) D. T. Shieh and B. J. Hwang, *Electrochim. Acta*, **38**, 2239 (1993); (b) L. A. da Silva, V. A. Alves, M. A. P. da Silva, S. Trasatti, and J. F. C. Boodts, *Can. J. Chem.*, **75**, 1483 (1997); (c) L. A. da Silva, V. A. Alves, M. A. P. de Silva, S. Trasatti, and J. F. C. Boodts, *Electrochim. Acta*, **42**, 271 (1997).
12. C. C. Waraksa, G. Chen, T. E. Mallouk, D. D. Macdonald, *J. Electrochem. Soc.*, **150**, E429 (2003).
13. *Handbook of Electrolyte Solutions Part A*, V. M. M. Lobo, Editor, Elsevier Science Publishers, B. V. (1989).
14. R. F. Bartholomew and D. R. Frankl, *Phys. Rev.*, **187**, 828 (1969).
15. (a) A. M. Sukhotin and L. I. Tungusova, in *Titanium Alloys*, Vol. 2, p. 891, J. C. Williams and A. F. Belov, Editors, Plenum, New York (1982); (b) A. M. Sukhotin and L. I. Tungusova, *Zashch. Metal.*, **7**, 654 (1971).
16. (a) D. C. Grahame, *Chem. Rev. (Washington, D.C.)*, **47**, 441 (1947); (b) L. I. Antropov, *Theoretical Electrochemistry*, Chap. 10, MIR Publishers, Moscow (1972).